



On the Salt Water Intrusion into the Durusu Lake, Istanbul: A Joint Central Loop TEM And Multi-Electrode ERT Field Survey

AYÇA SULTAN ARDALI,^{1,2}  BÜLENT TEZKAN,¹ and AYSAN GÜRER²

Abstract—Durusu Lake is the biggest and most important freshwater source supplying drinking water to the European side of Istanbul. In this study, electrical resistivity tomography (ERT) and transient electromagnetic (TEM) measurements were applied to detect a possible salt water intrusion into the lake and to delineate the subsurface structure in the north of Durusu Lake. The ERT and TEM measurements were carried out along six parallel profiles extending from the sea coast to the lake shore on the dune barrier. TEM data were interpreted using different 1-D inversion methods such as Occam, Marquardt, and laterally constrained inversion (LCI). ERT data were interpreted using 2-D inversion techniques. The inversion results of ERT and TEM data were shown as resistivity depth sections including topography. The sand layer spreading over the basin has a resistivity of 150–400 Ωm with a thickness of 5–10 m. The sandy layer with clay, silt, and gravel has a resistivity of 15–100 Ωm and a thickness of 10–40 m followed by a clay layer of a resistivity below 10 Ωm . When the inversion of these data is interpreted along with the hydrogeology of the area, it is concluded that the salt water intrusion along the dune barrier is not common and occurs at a particular area where the distance between lake and sea is very close. Using information from boreholes around the lake, it was verified that the common conductive region at depths of 30 m or more consists of clay layers and clay lenses.

Key words: Transient electromagnetic method, electrical resistivity tomography, salt water intrusion.

1. Introduction

From the beginning of life, water is an indispensable need for the survival of living things. The overconsumption of groundwater caused by the increasing population, as well as by industrial,

agricultural, and urban water needs, is leading to the degradation of the natural and sensitive balance between freshwater and salt water in the coastal regions thus causing the salt water to move inland. Therefore, it is important to derive information about the salt water intrusion at the coastal areas. Our investigation area is the Durusu Lake Basin on the Black Sea coast region near the large city of Istanbul. Durusu Lake, which is of lagoon origin and has an average depth of 4.5 m, holds 22% of the fresh water reserves around Istanbul. It supplies a significant portion of drinking water to Istanbul. There is a narrow and a low dune barrier separating Durusu Lake from the Black Sea. This barrier was formed by sands accumulated by the Black Sea at the place where several rivers converged and drained into the sea. It is known that the narrow dune barrier is eroding because of beach tides and sand supply (ISKI 2009). The formation of the lake is related to the development of a dune barrier separating the lake from the Black Sea. Because of the lake's importance as a drinking water supply, it is urgent to reveal the characteristics of the subsurface system of the narrow coast line between the lake and the Black Sea. In the eastern region, the thickness of the sand between sea and lake is too thin.

It is important to understand the hydraulic relation between the lake and the sea and to determine the location of the possible salt water wedge in terms of protecting the critical balance in the basin. For this purpose, electrical resistivity tomography (ERT) and transient electromagnetic (TEM) measurements were applied to detect a possible salt water intrusion and to delineate the subsurface structure north of Durusu Lake. The ERT and TEM methods are chosen, because they are frequently used in the geophysical

¹ Institute of Geophysics and Meteorology, University of Cologne, Albertus-Magnus Platz, 50923 Cologne, Germany. E-mail: aardali@uni-koeln.de; aycasardali@gmail.com; tezkan@geo.uni-koeln.de

² Istanbul University, Istanbul, Turkey. E-mail: agurer@istanbul.edu.tr

characterization of aquifers such as the interface of salt–fresh water, the distinction of sand–clay and the depth of the groundwater table (Goldman et al. 1991; Kruse et al. 1998; Hodlur et al. 2006; Wilson et al. 2006; Chongo 2011).

The TEM method is based on the change of the vertical conductivity of the ground composed of direction-independent horizontal layers, while the ERT method is based on vertical and horizontal resistivity changes (Spies and Frischknecht 1991). Additionally, they are commonly used to map salt water intrusion at coastal areas (Urish 1990; Ebraheem et al. 1997; Nowroozi et al. 1999; Nassir 2000; Choudhury et al. 2004; Kafri et al. 2005; Mitsuhata 2006; Sherif et al. 2006; Kafri et al. 2007; Nguyen 2009; Ezersky 2011).

The ERT and TEM measurements were carried out along six parallel profiles extending from the sea coast to the lake shore on the dune barrier that separates the lake from the sea. The resistivity cross-sections from the inversion of ERT data were used to investigate the 2-D resistivity distribution in the area. The TEM method was used for the first time in the region. TEM data were interpreted using different 1-D inversion techniques. The inversion of these data leads to the conclusion that the salt water intrusion along the barrier is not common. The salt water intrusion might occur at a particular area where the distance between the lake and the sea is very close (165 m). Because the Durusu Basin lies within the protection area, there are only few borehole data available for groundwater and geotechnical surveys. Using the information from the boreholes around the lake, it was verified that the common conductive regions on other profiles were made up of clay levels and clay lenses. These clay lenses are preventing a rapid water loss from the lake to the sea and are slowing down the salt water intrusion, too. This study revealed the place of clay lenses at the lake system and the influence of clay lenses on the water cycle by geoelectrical images.

2. Geology and Hydrogeology of Durusu Basin

The geology of the basin is given according to the previous drillings within the context of groundwater

and dam site surveys (AVES 2009) and hydrogeological studies (ISKI 2009) as well as the studies of MTA (Çağlayan et al. 1998) (Fig. 1). The lake consists of Eocene limestone and marls and Neogene sand and gravel sequences covering them, and it lies at the edge of a morphological elevation of 100–150 m. Due to the formation process, the Durusu Lake is an ancient bay where many rivers meet. In Quaternary, the bay was closed because of transgression, and the Durusu Lake was formed. Due to the morphological structure of the Durusu Lake, it is very indented and protruding, so there are many large and small rivers reaching the lake.

The formations in the research area and the Durusu Basin, from older to younger units are Ihsaniye Formation, Ergene Formation, Marine Sediments, and Alluvium (Fig. 1). The thickness of Alluvium changes from 200 to 2800 m. The permeable zone consists of sand, sand with clay, and sandstone. The impermeable zone consists of clay, marl, and clay with silt. The wideness between the sea and the lake changes from 0.2 to 3.7 km. There is a beach lying parallel to the coastline which has a width of 20–50 m. There was not much borehole data for groundwater and geotechnical surveys around the Durusu Lake, so the borehole information in the basin was processed on the geological map. The cross-sections were prepared using the borehole information (Fig. 1). According to the information from the few boreholes around Durusu Lake, the Ergene Formation at the northern part of the basin includes sand with gravel, clay, sandstone, and claystone; the Ihsaniye Formation at the southern part of the basin includes clay, sand, claystone, and sandstone with clay interbeds; the Marine sediments at the sea coast include sand with clay and gravel (AVES 2009; ISKI 2009; AYB 2004) (Fig. 1).

The Karacaköy boreholes, which were drilled on the Ergene Formation with an interval of 300–500 m, have clay layers at a depth of 50–150 m (Fig. 1a). However, these layers cannot be monitored in some neighboring boreholes. So, these clay layers are probably clay lenses. According to lithology, a significant portion of the Hisarbeyli boreholes on the Ihsaniye formation consists of clay and mudstone. Some Hisarbeyli boreholes contain gravel and very thin clay lenses (Fig. 1b). Generally, these boreholes

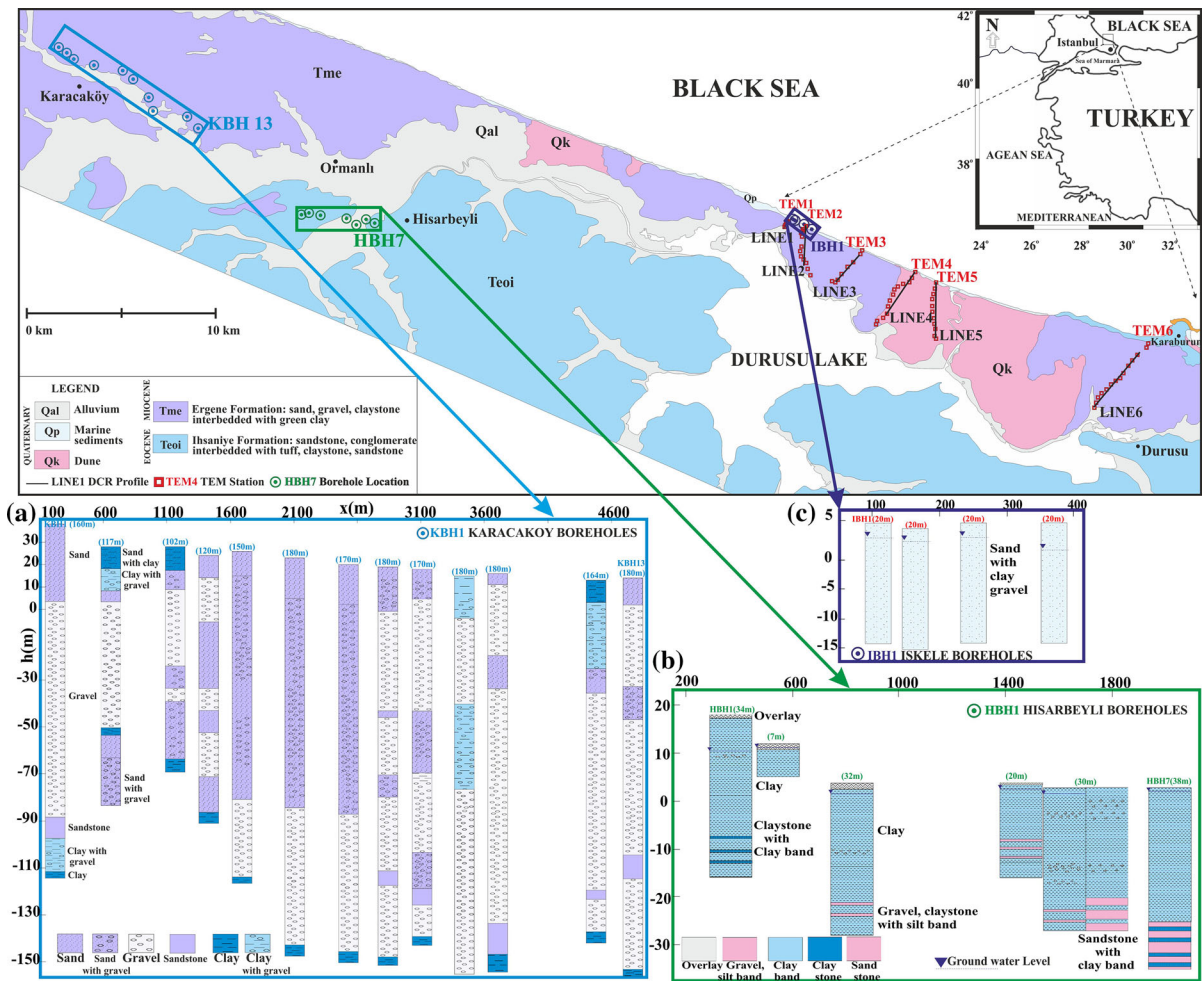


Figure 1

The borehole locations, geophysical profiles are shown on the geology map (Çağlayan et al. 1998) of the Durusu Basin, showing **a** Karacaköy boreholes on Ergene Formation **b** Hisarbeyli boreholes on Ihsaniye Formation **c** Iskele boreholes on marine sediments

do not exceed a depth of 40 m. While the Ihsaniye Formation is dominated by clay and claystone at the first 30 m, sand and gravel are predominant at the survey area in the Ergene Formation. This situation makes the bottom of the lake impermeable, because it is located mostly on clay units of the Ihsaniye Formation. Some bottom parts of the lake are located on the Ergene formation. Although clay bands and lenses of this formation contribute to the protection of the lake water, the unit usually contains permeable sand and gravel. Marine sediments, which include sand with clay and gravel, were observed at Iskele Boreholes between 0 and 20 m depth (Fig. 1c). There is a base of permeable and rock environment in the

SW of the Durusu Basin. The semipermeable part in the NW and SE borders the aquifer environment of the basin. This condition causes the shaping of a hydrogeologic environment of “Unconfined Aquifer” in the SW of the Durusu Basin.

3. The Interpretation of TEM Data

The TEM measurements were carried out at 63 stations along six parallel profiles extending from the sea coast to the lake shore using the NT-20 transmitter and the GDP- 32II receiver from Zonge Engineering (Zonge 2002). The distance between

neighboring TEM stations varies between 20 and 350 m at greater distances. At the TEM stations, the central loop configuration was applied using $20 \times 20 \text{ m}^2$ ($50 \times 50 \text{ m}^2$ transmitter loops where adequate areas are available) transmitter loops and $5 \times 5 \text{ m}^2$ receiver coils. Using the central loop configuration, the NanoTEM mode for shallow investigations was operated with a current of 3 A and the ZeroTEM mode for deeper investigations with a current of 9 A. The transmitter turn-off time (ramp-time) depends primarily on the current and loop size. For the applied field configuration, the ramp-time was $1.5 \mu\text{s}$ in NT mode and $20 \mu\text{s}$ in ZT mode. The induced voltages were recorded in the time range of $0.3 \mu\text{s}$ – 1 ms in the NT mode and in the time range of $40 \mu\text{s}$ – 6 ms in the ZT mode. The end of the ramp-time is defined as $t = 0$ for the Zonge TEM system. At each station, both modes were employed resulting in two transients. Noise measurements were also carried out at every profile once a day. This procedure is, according to our experience, sufficient and the observed noise data represent the noise level of each TEM survey day. A stacking algorithm was applied to improve the signal to noise ratio at every TEM station. Afterwards, a deconvolution algorithm was applied to remove the influence of the nonzero transmitter turn-off time (Lange 2003; Helwig et al. 2003) and to merge the transients to one (von Papen et al. 2013; Sudha et al. 2010; Yogeshwar et al. 2013; Yogeshwar 2014). In Fig. 2, a non-deconvolved NT and ZT data with the deconvolved and stitched NT/ZT data are shown for the station T5 of the profile TEM3. Figure 2b demonstrates all the measured NT/ZT transients together with the measured noise for the ZT mode. As shown by Yogeshwar et al. 2013, there are only marginal differences between 1D inversion results of the deconvolved and non-deconvolved data. The induced voltage data of the TEM3 profile beneath the measured noise level ($t > 10^{-3} \text{ s}$) were not used in the inversion procedure. TEM data were transformed from induced voltages into late-time apparent resistivities. A 1-D inversion approach using Occam and Marquardt methods was used. The Occam inversion method with first- and second-order smoothness constraints generates a smooth resistivity-depth model from the measured data with a predefined misfit value (Constable et al. 1987). The

depth of divergence of the two Occam inversion results, which can be used to validate a minimum and maximum depth of investigation, is interpreted as the initial model for the Marquardt inversion. Instead of minimizing only the cost function of the data Φ_d , the length of the model update is also minimized in the Marquardt inversion. The total cost function reads

$$\Phi = \Phi_d + \lambda \Phi_m \rightarrow \min \quad (1)$$

where Φ_m is the model cost function. The λ is a Lagrange multiplier and weights between the only data-based functional Φ_d and the step-size of the model update Φ_m . The equivalent models were calculated using the Monte Carlo algorithm (Scholl 2005) to show the best-fit with 1-D Marquardt models (Fig. 3a). The quality of fitting is, thereby, determined through the root-mean-square error defined as:

$$\text{RMS} = \sqrt{\frac{1}{N} \sum_{i=1}^N \left(\frac{d_i - f_i}{d_i} \right)^2} \times 100 \quad (2)$$

with the measured data d_i , the forward calculation f_i , and the number of time points N . The importance values were calculated using singular value decomposition (SVD) of the Jacobian (G) to determine the parameter resolution defined as a value of 1 for well-resolved model parameters (Menke 1984). The Jacobian

$$G = USV^T \quad (3)$$

where the matrix U maps from data to model space and matrix V maps within model space. The diagonal matrix $S_{ij} = \tau_{ij} s_i$ (where τ_{ij} denotes the Kronecker delta) contains the singular values (s_i) of the Jacobian, which are used to calculate the so-called ‘importances’ of the parameters. This can be done with a damping matrix

$$T_{ij} = \tau_{ij} \frac{\hat{s}_i^2}{\hat{s}_i^2 + \hat{\epsilon}^2} \quad (4)$$

where $\hat{s}_i = s_i/s_{\text{max}}$ are the singular values normalized to the maximum singular value s_{max} of the Jacobian and $\hat{\epsilon}$ is the so-called singular value threshold. The damping matrix can be introduced into the inversion process equivalently to the damped Marquardt inversion (Vozoff and Jupp 1975). The importances are calculated by transforming the normalized

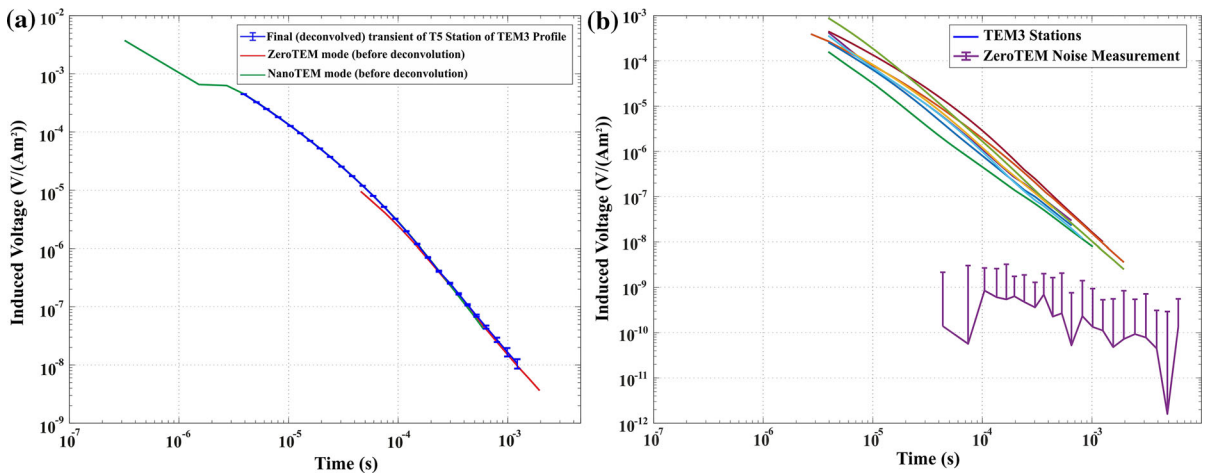


Figure 2

a The deconvolved transient of data taken at station T5 of the TEM3 profile together with measured transients before deconvolution for NanoTEM and ZeroTEM modes. **b** The measured noise level of ZeroTEM mode and the induced voltage data of all stations of the TEM3 profile

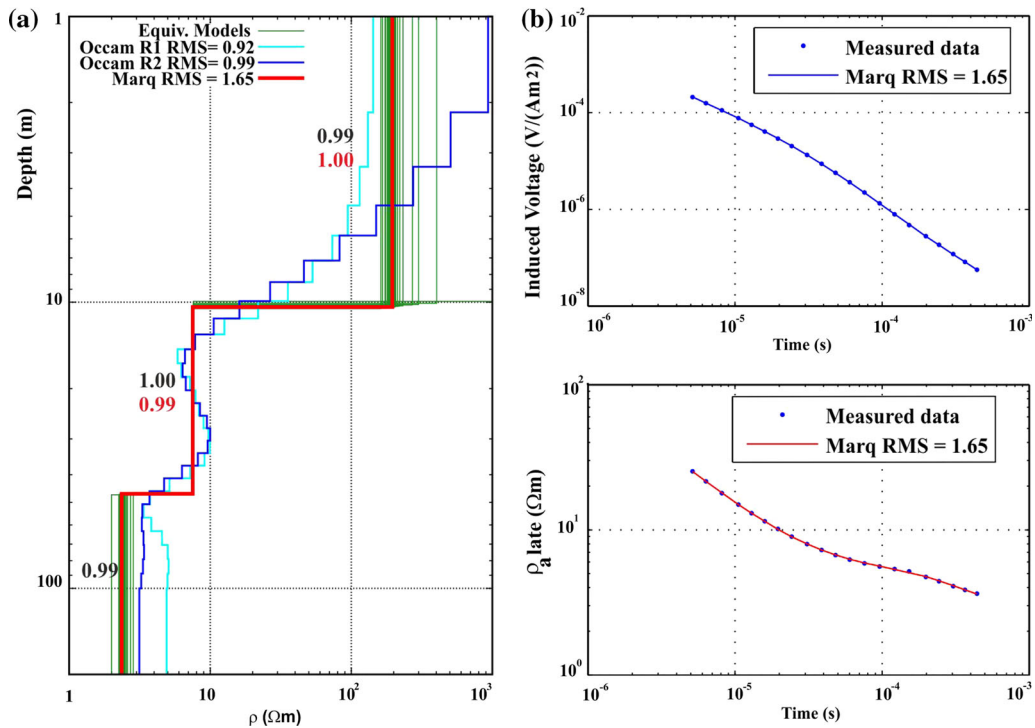


Figure 3

The inversion results of the T3 station of the TEM3 profile, showing **a** 1-D Occam, Marquardt and equivalent models with importance values of **b** measured and calculated data

singular values to model parameter space giving an importance I_i , which ranges from zero to one, zero standing for no resolution and one for perfect resolution. The exact formula is:

$$I_i = \sum_{i=1}^M \left| v_{ii} \frac{s_i^2}{s_i^2 + \varepsilon_1^2} \right| \quad (5)$$

where M is the number of model parameters, v_{ii} is the corresponding component of the model transformation matrix V obtained from the SVD and the threshold is fixed to $\varepsilon_1 = 0.01$ (von Papen et al. 2013). The inversion result for the T3 station of the TEM3 profile was given as an example (Fig. 3). It shows that the model is resolved up to a depth of 50 m and can be represented by a three-layer case. The results of the Occam inversion are used to perform a Marquardt inversion. According to the model parameter, the importances of the TEM models, the resistivities of all three layers, and the depths are well-resolved. The processed TEM data for the T3 station of the TEM3 profile is presented in Fig. 3b as apparent resistivities. The results of the Occam inversions of TEM data for all profiles were shown as quasi 2-D model sections including the topography at a single color scale (Fig. 4). After stitching together the 1-D inversion results of the TEM stations, the triangulation and linear interpolation techniques were applied to the resistivity, to the depth, and to the station distances to plot the geoelectric cross-sections. The geological interfaces are shown on these resistivity-depth sections as white dashed lines using the information from the hydrogeology and the boreholes of the area.

The sand layer spreading over the basin has a resistivity of 150–400 Ωm with a thickness of 5–10 m. The medium layer has a resistivity of 15–100 Ωm and a thickness of 10–40 m, followed by a very conductive clay layer of a resistivity below 10 Ωm . In addition, the importance parameters of each station were displayed in Fig. 4.

Thus, the importances of the TEM stations show, generally, a good parameter resolution except for two or three stations at each profile. The high importance values of the second and third layers show a good correspondence with the models at the TEM profiles. The average root mean square (RMS) error of all

TEM profiles is 4%. The investigation depth of the TEM data was calculated about 60 m according to

$$\delta_{\text{doi}} \approx 0.55 \left(\frac{IA_{Tx}\bar{\rho}}{\eta_v} \right)^{\frac{1}{5}} \quad (6)$$

for central loop TEM soundings in the near zone (late times) (Spies 1989). I is the current, A_{Tx} is the size of the transmitter loop and η_v is the measured voltage noise level. A typical value for TEM soundings in the survey area is 3×10^{-8} V/Am² (see Fig. 2). ρ is the average resistivity estimated by the average resistivity of the first three layers of the model at the corresponding point. The δ_{doi} is estimated from final 1-D inversion models and plotted as a lower depth bound. Therefore, the thickness of the conductive clay layer could not be determined beyond this depth. Unlike other profiles, the very conductive layer ($< 4 \Omega\text{m}$) above the DOI at TEM1 profile could indicate a possible salt water intrusion.

4. Laterally Constrained Inversion (LCI) of TEM Data

Smooth lateral variations of conductivity were expected according to the Occam and Marquardt inversions. Therefore, LCI was applied on the TEM data additionally. The laterally constrained inversion scheme is described in detail by Auken and Christiansen (2004). The LCI is a parametrized inversion of data of the same type with lateral constraints on the model parameters between neighboring models (Auken et al. 2005). The lateral distances between the 1-D models are determined by the sampling density of the data. The resulting model sections are laterally smooth with sharp layer interfaces as quasi 2-D model sections. As an example of all TEM profiles, the LCI model of the TEM5 profile with four layers was displayed in Fig. 5. The constraints between the resistivities and the depth interfaces have been set in a way allowing the parameters to vary in a range of 10%. The depth of investigation (DOI) was calculated according to Eq. 6 and was shown as a black line along the profile. There is a resistive layer on top which belongs to the sand formation (Fig. 5a). The resistive sand formation is followed by sand with

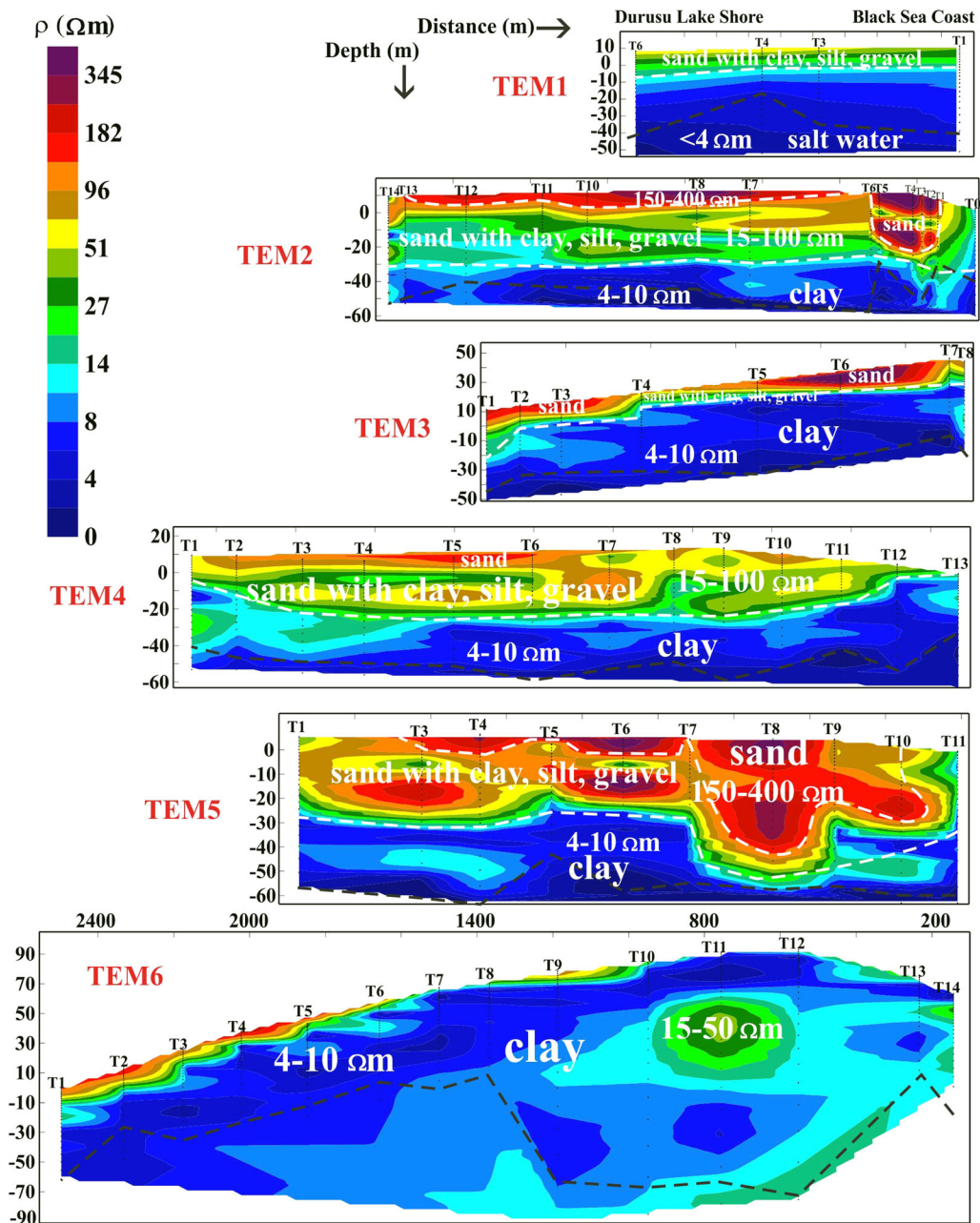


Figure 4

The interpolated resistivity cross-sections of 1-D Occam inversion models of TEM profiles at a single color scale with the depth of the investigation (black dashed lines)

clay, silt and gravel with 50–80 Ωm, and a thickness of 30 m. The very conductive third and fourth layers of the clay formation have a resistivity of about 4–10 Ωm at depths between 30 and 70 m. In Fig. 5b, the standard deviation factor (STDF) for the

parameter m_s , thickness and resistivities of each layer, and the RMS of each station mainly present well-determined parameters along the profile. Standard deviations on model parameters are calculated

$$STDF(m_s) = \exp(\sqrt{C_{est,ss}}) \quad (7)$$

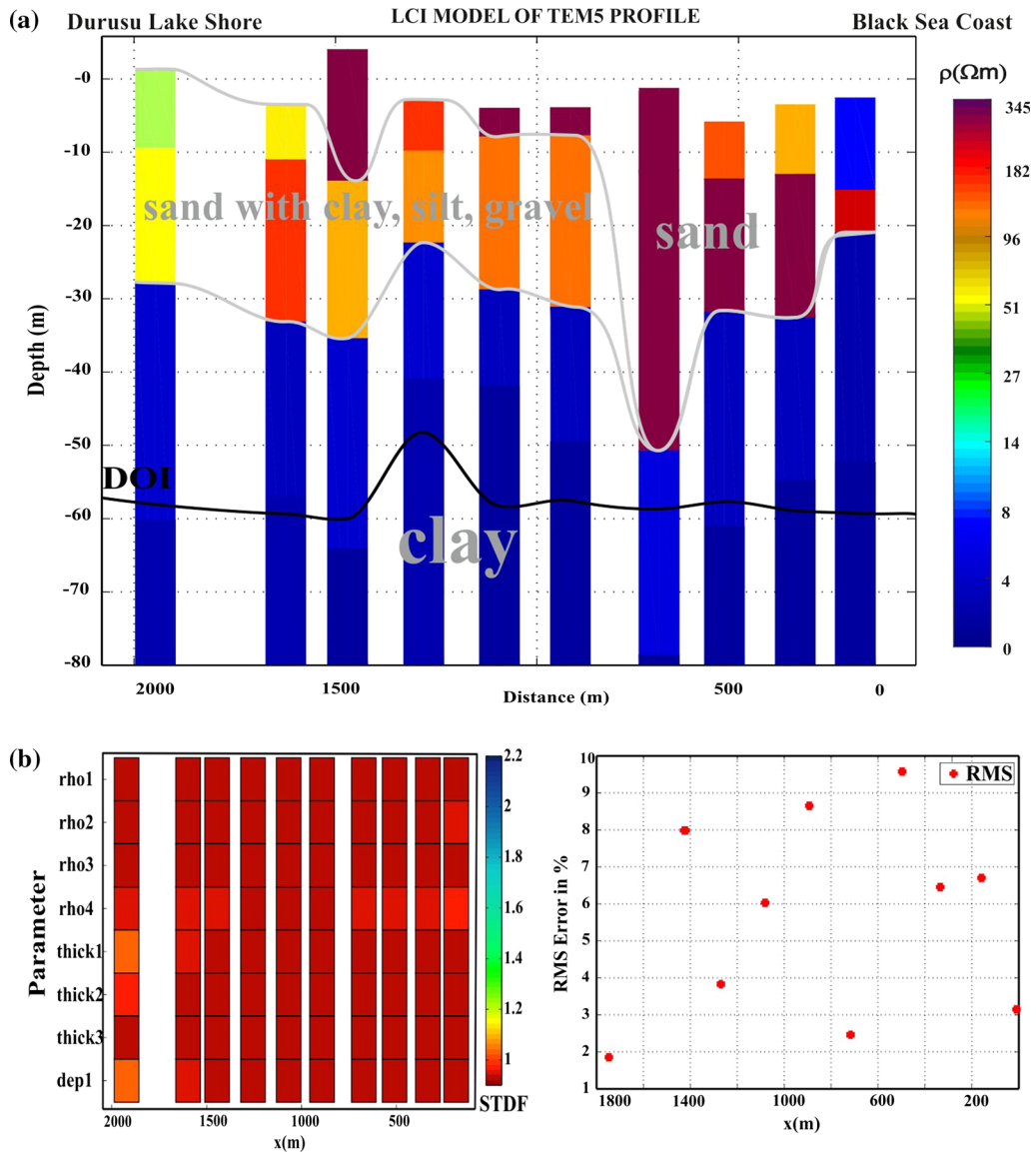


Figure 5

a The LCI model of the TEM5 profile b parameter analysis (STDF and RMS of each TEM station). The gray line shows the interface between the layers and the black line shows the depth of investigation

using the diagonal elements in C_{est} (the covariance of the estimation error). The theoretical case for the perfect resolution has $STDF = 1$; $STDF = 1.1$ is approximately equivalent to an error of 10%. Well-resolved parameters have $STDF < 1.2$, moderately resolved parameters $1.2 < STDF < 1.5$, poorly resolved parameters $1.5 < STDF < 2$, and

unresolved parameters $STDF > 2$ (Auken and Christiansen 2004).

5. The Interpretation of ERT Data

The ERT measurements were carried out along six parallel lines extending from the sea coast to the lake shore on the same profiles as for TEM (Ardali

2014). The multi channel ERT measurements consisting of the dipole–dipole configuration were applied using 56 electrodes with a spacing of 20 m. The 2-D inversion of ERT data was calculated by using the smoothness-constrained least-squares method with RES2DINV ver.3.4 (Geotomo Software).

The interpretation of the recovered 2-D resistivity sections of these data, along with the hydrogeology of the area, leads to the conclusion that the salt water intrusion along the barrier is not common. It is considered that the low resistivity values of 5–10 Ωm at depths between 40 and 100 m on the cross-sections are the clay lenses of the Ergene Formation (Fig. 6). This information is compatible with the Karacaköy boreholes which have clay layers at a depth of 50–150 m (Fig. 1a). As the Hisarbeyli boreholes are dominated by clay and claystone at the first 30 m, they are used to define the conductive clay lenses on geoelectrical cross-sections (Fig. 1b). The high resistivity values ($> 200 \Omega\text{m}$) belong to the sand layer covering the basin. The possible salt water intrusion occurs where the distance between the lake and the sea is very close, at the ERT profile of LINE1. By the sea coast of the LINE1 cross-section, very low resistivity values ($< 4 \Omega\text{m}$) were monitored within the sand layer at the first 20 m (Fig. 6). The marine sediments observed at the Iskele boreholes at depths of 0–20 m is well-matched with this information (Fig. 1c).

6. Discussion and Modeling Study

The inversion calculations of TEM and ERT data observed on the survey area indicate a conductive layer at a depth of 30 m with resistivities in average of 5–10 Ωm (Fig. 4 and 6) except LINE1 where the conductive layer as determined at a depth of 10 m, shows an average resistivity of less than 5 Ωm . The conductive layer can be interpreted as a clay layer, but it can be also interpreted as a possible salt water intrusion from the Black Sea. Using electrical and electromagnetic methods, it is sometimes not easy to define the clay layer and possible salt water intrusion, because they can have similar resistivity values. According to the borehole information from the

survey area, a clay layer is expected at a depth of 30 m. Therefore, we have taken a reference station which is far away (15 km) from the coast where the geology (the 20–30 m deep clay layer)—according to the boreholes—was assumed not to have changed. No salt water intrusion is expected at this station which is far away from the Black Sea coast. The 1D inversion of these TEM data gives a clear indication of a relatively conductive layer at about 30 m depth with a resistivity of about 10 Ωm . According to the inversion statistics, the resistivity of this last layer is well-resolved. However, the resistivity of it is comparable to the resistivity of the survey area at the same depth. It is also difficult to interpret the good conductive layer as a salt water intrusion with the help of the reference station. The TEM1 profile is an exception, where a good conductive structure ($< 4 \Omega\text{m}$) was determined at approximately 30 m depth (Figs. 4 and 6).

The resistivity of the last layer for the TEM1 stations is also well-resolved according to the importances (0.9 with Eq. 5) and according to the STDF. However, the resolution of the resistivity of the last layer of the survey area is also crucial for the interpretation of the salt water intrusion. Therefore, a modeling study was carried out, as an example, for the T3 station of the TEM1 profile to examine the resolution of the resistivity of this layer (Fig. 7). From the inversion of the T3 station of the TEM1 profile, the resistivity of the last layer was determined as 4 Ωm , and a relative good fitting (RMS = 2.71%) was also obtained. We realized forward modeling calculations by changing the resistivity of the last layer (ρ_3 , Fig. 7a) to 1, 10, and 20 Ωm , while other model parameters were fixed. Figure 7c shows the calculated late time apparent resistivity data for each model and their corresponding model fitting. The RMS values are clearly increasing due to having changed the resistivity of the last layer (Fig. 7c).

A similar modeling study was carried out with the 2-D ERT model of LINE1. A very conductive last layer ($< 4 \Omega\text{m}$) was also detected using the 2-D inversion with a RMS of 5% (Fig. 8b). A systematic change of the resistivity from 1 to 30 Ωm indicates that the RMS will be worse if the resistivity of the last layer increases or decreases. An example of this modeling study is demonstrated in Fig. 8c where the

Durusu Lake Shore

Black
Sea Coast

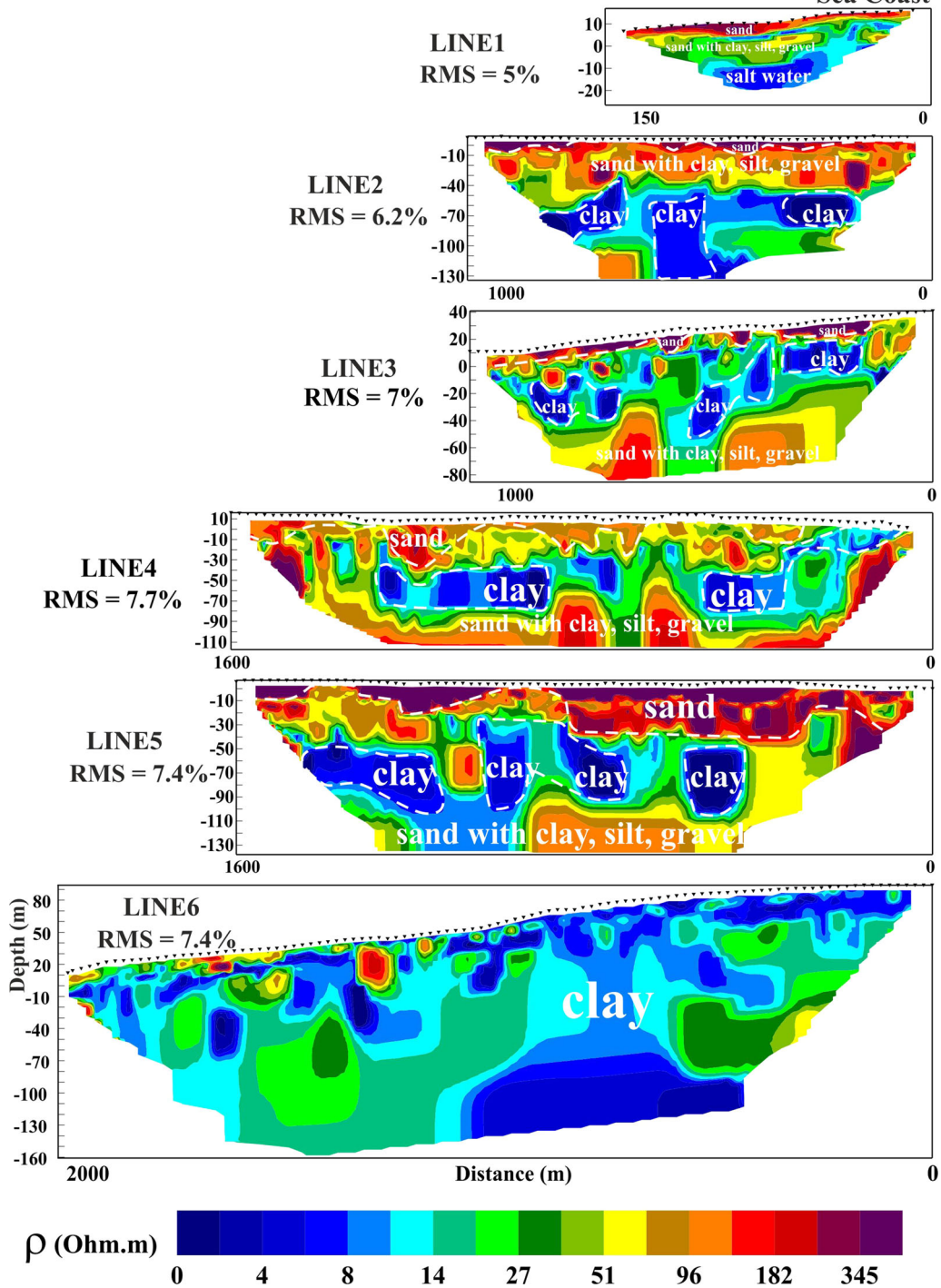


Figure 6

The presentation of the resistivity values of the 2-D inversion of ERT profiles at a single color scale

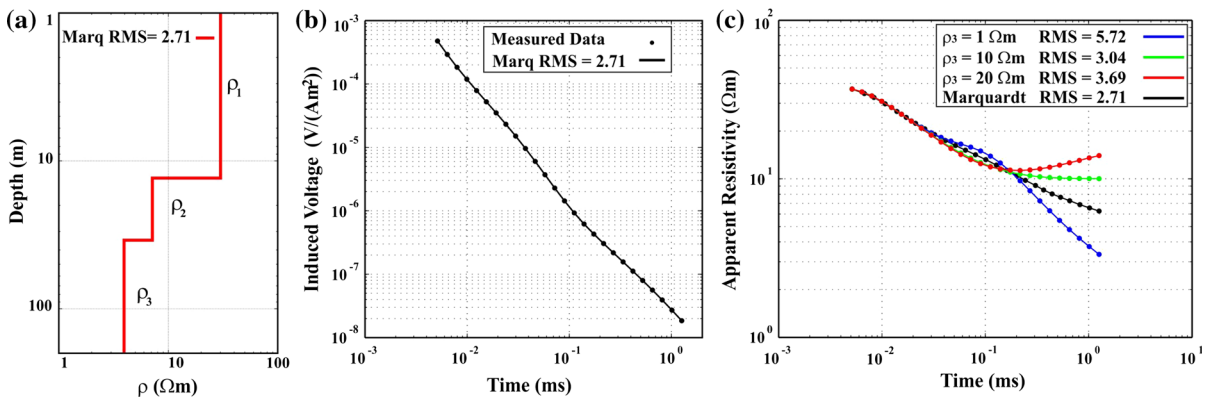


Figure 7

a The inversion result of b the induced voltage data of c 1-D forward calculations with the resistivity of the last layer 20 Ωm; 10 and 1 Ωm is compared with the T3 station of the TEM1 profile

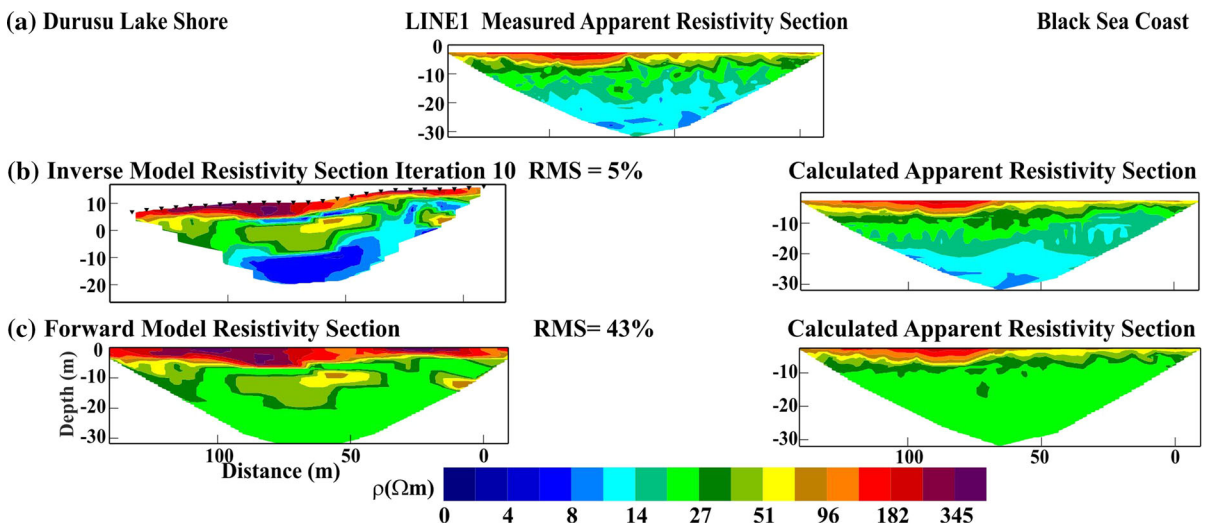


Figure 8

2-D modeling study for LINE1 showing the sections a measured apparent resistivity b 2-D inversion and the calculated apparent resistivity c 2-D alternative conductivity model and calculated apparent resistivity

resistivity of the last layer is assumed as 20 Ωm and the other model parameters of the 2-D ERT model remain unchanged. A high RMS error of 43% indicates that a more conductive layer than 20 Ωm should be expected for the last layer.

The modeling studies for ERT and TEM models confirm that a conductive layer with resistivities less than 10 Ωm should exist beneath the survey area at about a depth of 30 m. The resistivity of this layer is less than the resistivity of the Reference Station. However, the geophysical modeling results are not

clear enough to interpret the relatively conductive layer of profiles TEM2–TEM6 as the salt water intrusion. We have interpreted it as clay lenses according to the boreholes (Figs. 4, 6). The only exception is TEM1 profile where a good conductive layer was detected at depths less than 10 m. According to the boreholes, a sandy layer is also expected there.

The clay lenses observed on the ERT lines were not seen on the TEM profiles. The clay layer is not a continuous layer as derived from the TEM inversion.

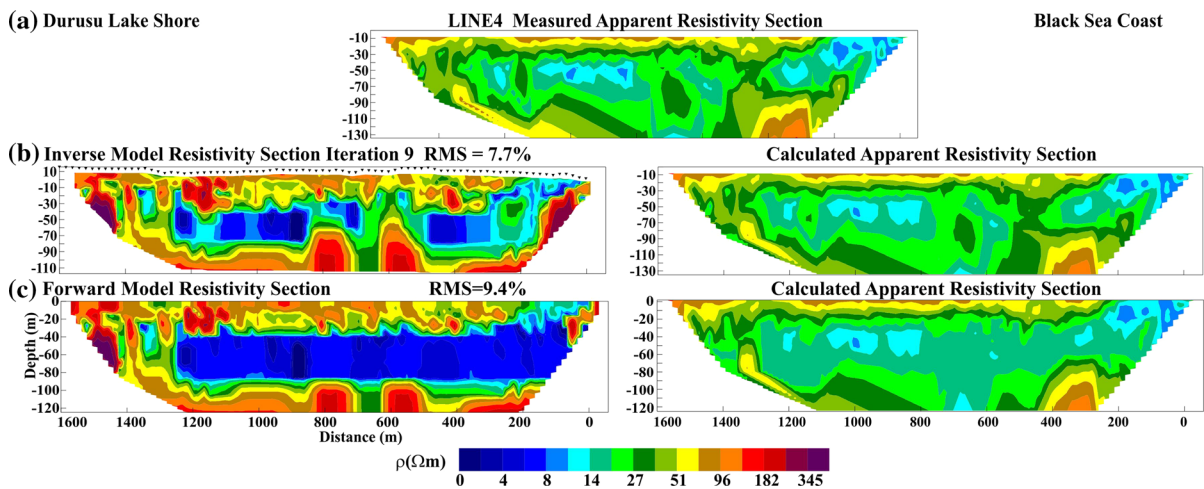


Figure 9

2-D modeling study for LINE4 to study the equivalence problem showing the sections **a** measured apparent resistivity **b** 2-D inversion and the calculated apparent resistivity **c** 2-D alternative conductivity model and calculated apparent resistivity

It appears as a clay lens interrupted by resistive formations. To study whether the occurrence of clay lenses in the ERT inversion is an artifact of the 2-D inversion or not, a modeling study was carried out. Synthetic data for dipole–dipole configuration was generated for a forward model of a conductive layer sandwiched between two layers of higher resistivities. The result of the modeling study is demonstrated in Fig. 9 for LINE4. In this modeling study, all model parameters in the 2-D ERT model were fixed (Fig. 9b); only the clay layer was assumed as a continuous layer (Fig. 9c). The RMS of the 2-D inversion is 7.7% (Fig. 9b), the RMS of the forward model is 9.4% (Fig. 9c) indicating that the conductive layer is laterally not continuous. A better RMS error can only be achieved if the clay layer is not continuous. The inversion of the measured apparent resistivity data resulted in individual conductive structures. They can also be determined as clay lenses all according to the 2-D ERT inversion result (Fig. 9b). Because of the large distance and due to the interpolation between the 1-D inversion results of the neighboring TEM stations, the clay layer was interpreted as a continuous layer (Figs. 7 and 5).

7. Conclusions

In this study, the possible salt water intrusion from the Black Sea to the Durusu Lake was investigated for the first time using multichannel ERT and central loop TEM methods. The ERT and TEM measurements were carried out along six parallel profiles extending from the sea coast to the lake shore. The inversion models of geoelectrical data were shown as geoelectrical cross-sections.

At the geoelectrical cross-sections of ERT lines and TEM profiles, three layers were identified. The first two layers observed on the ERT sections correspond to the resistivity properties of the three layers determined in the TEM sections. Because of the large distance and due to the interpolation between the TEM stations, the conductive layer at about a depth of 30 m was interpreted as continuous along the profiles. The LCI models show, at the same depths as the 1-D Marquardt models, a good correspondence with the resistivity values. The dune formation spreading over the study area has high resistivity values at shallow depths. There are individual conductive structures determined as clay lenses in the middle of the ERT resistivity sections. This conductive unit of clay lenses belongs to the Ergene

Formation under the dune formation. A unit of sand with conglomerate is underlying the clay lenses.

When the geoelectrical models obtained in this study are evaluated together with topography, borehole, and geological data, an approach can be made for the Durusu Lake subsurface system. It is evident that the topography along the geoelectrical profiles is declining from the lake to the sea. A large part of the lake is on the Ihsaniye Formation and is composed of clay lenses with resistivity values between 4 and 10 Ωm at the first 30 m. The northern part is located on the Ergene Formation which consists of clay, clay with gravel, sand with clay, and gravel with resistivity values of 4–10 Ωm at depths between 40 and 100 m. In the vicinity of the lake, alluviums feeding the lake are seen along the riverbeds.

The geoelectrical studies showed that a widespread salt water intrusion may not exist near the Durusu Lake which had a shoreline next to the sea. A restricted sea water intrusion exists in the region along the 2-D ERT profile of LINE1 which has the shortest distance between the lake and the sea (165 m). On the sea coast of the LINE1 profile, very low resistivity values ($< 4 \Omega\text{m}$) of the sand layer were observed at a depth more than 20 m belonging to the marine sediments of the Iskele boreholes. The inversion of the measured apparent resistivity data resulted in individual conductive structures determined as clay lenses in the middle of the ERT resistivity sections. The clay lenses at a depth of about 30 m observed on ERT lines were not seen on TEM profiles because of the large distance between the stations and because of the interpolation of the 1-D TEM inversion results of neighboring TEM stations. These very conductive clay lenses may be acting as natural barriers that prevent a rapid water movement from sea to land and opposite, to protect the Durusu Lake.

Acknowledgements

The authors would like to thank all helpers during the field survey, especially Juliane, Jan, and my brother Arda as well as Amir, Klaus, and Pritam for their great support in interpreting the TEM data. This work was supported by Scientific Research Projects (BAP-

80624) of Istanbul University and The Scientific and Technological Research Council of Turkey (TUBITAK) 2214, Research Fellowship Programme for Ph.D. Students. TEM measurements were applied using the Nanotem equipment and the 1-D inversion of TEM data was done with the support of the Institute for Geophysics and Meteorology of the University of Cologne.

REFERENCES

- Ardali, A.S. (2014) Investigation of salt water intrusion in terkos basin using transient electromagnetic and direct current resistivity methods. Ph.D. thesis, Istanbul University, Turkey.
- Auken, E., & Christiansen, A. V. (2004). Layered and laterally constrained 2D inversion of resistivity data. *Geophysics*, 69, 752–761.
- Auken, E., Christiansen, A. V., Jacobsen, B. H., Foged, N., & Sorensen, K. I. (2005). Piecewise 1D laterally constrained inversion of resistivity data. *Geophysical Prospecting*, 53, 497–506.
- AVES, (2009) The planning report of terkos additional reservoir.
- AYB, (2004) The report of terkos çakıl harbour.
- Çağlayan, M.A. and Yurtsever A. (1998) The 1/100 000 scaled maps' series of MTA.No:20,21,22, 23.
- Chongo, M. (2011). The use of time domain electromagnetic method and continuous vertical electrical sounding to map groundwater salinity in the barotse sub-basin, Zambia. *Physics and Chemistry of the Earth*, 36, 178–805.
- Choudhury, K., & Saha, D. K. (2004). Integrated geophysical and chemical study of saline water intrusion. *Ground Water*, 42, 671–677.
- Constable, S. C., Parker, R. L., & Constable, C. G. (1987). Occam's inversion: a practical algorithm for generating smooth models from electromagnetic sounding data. *Geophysics*, 52, 289–300.
- Ebraheem, M., Senosy, M., & Dahab, K. A. (1997). Geoelectrical and hydrogeochemical studies for delineating groundwater contamination due to salt-water intrusion in the northern part of the Nile Delta, Egypt. *Ground Water*, 35, 216–222.
- Ezersky, M. (2011). TEM study of the geoelectrical structure and groundwater salinity of the Nahal Hever sinkhole site, Dead Sea shore, Israel. *Journal of Applied Geophysics*, 75, 99–112.
- Goldman, M., Gilad, D., Ronen, A., & Melloul, A. (1991). Mapping of seawater intrusion into the coastal aquifer of Israel by the time domain electromagnetic method. *Geoexploration*, 28(2), 153–174.
- Helwig, S.L., Lange, J. and Hanstein, T. (2003) Kombination dekonvolvierter Messkurven zu einem langen Transienten. Tagungsaband der 63. Jahrestagung der Deutschen Geophysikalischen Gesellschaft, 44–45.
- Hodlur, G. K., Dhakate, R., & Andrade, R. (2006). Correlation of vertical electrical sounding and borehole log-data for delineation of saltwater and freshwater aquifers. *Geophysics*, 71, G11–G20.
- ISKI (2009) The business report for the agricultural sector of analytical studies in Istanbul metropolitan development plan. Istanbul metropolitan municipality directorate of planning and development Department of City Planning.

- Kafri, U., & Goldman, M. (2005). The use of the time domain electromagnetic method to delineate saline groundwater in granular and carbonate aquifers and to evaluate their porosity. *Journal of Applied Geophysics*, 57(3), 167–178.
- Kafri, U., Goldman, M., Lyakhovskiy, V., Scholl, C., Helwig, S., & Tezkan, B. (2007). The configuration of the fresh–saline groundwater interface within the regional Judea Group carbonate aquifer in northern Israel between the Mediterranean and the Dead Sea base levels as delineated by deep geoelectromagnetic soundings. *Journal of Hydrology*, 344, 123–134.
- Kruse, S. E., Brudzinski, M. R., & Geib, T. L. (1998). Use of electrical and electromagnetic techniques to map seawater intrusion near the Cross-Florida Barge Canal. *Environmental and Engineering Geoscience*, 4, 331–340.
- Lange, J. (2003) Joint Inversion von central-loop TEM und long-offset TEM transienten am beispiel von Messdaten aus Israel. Master's thesis, University of Cologne, Germany.
- Menke, W. (1984). *Geophysical data analysis: discrete inverse theory*. Orlando: Academic Press Inc.
- Mitsuhashi, Y. (2006). Various-scale electromagnetic investigations of high-salinity zones in a coastal plain. *Geophysics*, 71(6), B167–B173.
- Nassir, A. (2000). Salt-water intrusion mapping by geoelectrical imaging surveys. *Geophysical Prospecting*, 48, 647–661.
- Nguyen, F. (2009). Characterization of seawater intrusion using 2D electrical imaging. *Near Surface Geophysics*, 7, 377–390.
- Nowroozi, A. A., Horrocks, S. B., & Henderson, P. (1999). Salt-water intrusion into the freshwater aquifer in the eastern shore of Virginia: a reconnaissance electrical resistivity survey. *Journal of Applied Geophysics*, 42, 1–22.
- Scholl, C. (2005) The influence of multidimensional structures on the interpretation of LOTEM data with one-dimensional models and the application to data from Israel. Ph.D. thesis, University of Cologne, Germany.
- Sherif, M., El Mahmoudi, A., Garamoon, H., & Kacimov, A. (2006). Geoelectrical and hydrogeochemical studies for delineating seawater intrusion in the outlet of Wadi Ham, UAE. *Environmental Geology*, 49, 536–551.
- Spies, B. R. (1989). Depth of investigation in electromagnetic sounding methods. *Geophysics*, 54, 872–888.
- Spies, B. R., & Frischknecht, F. C. (1991). Electromagnetic sounding. In M. N. Nabighian (Ed.), *Electromagnetic methods in applied geophysics* (Vol. 2, pp. 285–425). Tulsa: Society of Exploration Geophysicists.
- Sudha, Tezkan, B., Israil, M., Singhal, D. C., & Rai, J. (2010). Geoelectrical mapping of aquifer contamination: a case study from Roorkee, India. *Near Surface Geophysics*, 8, 33–42.
- Urish, D. W., & Fröhlich, R. K. (1990). Surface electrical resistivity in coastal groundwater exploration. *Geoexploration*, 26, 267–289.
- von Papen, M., Tezkan, B., & Israil, M. (2013). Characterization of an aquifer in Roorkee, India using the spatially constrained inversion of in-loop TEM data. *Near Surface Geophysics*, 11, 85–94.
- Vozoff, K., & Jupp, D. L. B. (1975). Joint inversion of geophysical data. *Geophysical Journal of the Royal Astronomical Society*, 42, 977–991.
- Wilson, S. R., Ingham, M., & McConchie, J. A. (2006). The applicability of earth resistivity methods for saline interface definition. *Journal of Hydrology*, 316, 301–312.
- Yogeshwar, P. (2014) A resistivity-depth model of the central Azraq basin area, Jordan: 2D forward and inverse modeling of time domain electromagnetic data. Ph.D. thesis, Universität zu Köln, Institut für Geophysik und Meteorologie.
- Yogeshwar, P., Tezkan, B., & Haroon, A. (2013). Investigation of the Azraq sedimentary basin, Jordan using integrated geoelectrical and electromagnetic techniques. *Near Surface Geophysics*, 11, 283–291.
- Zonge M. (2002) GDP-32 II multi functional receiver operation manual. Zonge engineering and research organisation. <http://www.zonge.com/RxManuals.html>.

(Received August 8, 2017, revised February 15, 2018, accepted February 21, 2018, Published online February 28, 2018)